JACS
JOURNAL OF THE AMERICAN CHEMICAL SOCIETY
pubs.acs.org/JACS
Article

Turnover and Inactivation Mechanisms for (*S*)-3-Amino-4,4-difluorocyclopent-1-enecarboxylic Acid, a Selective Mechanism-Based Inactivator of Human Ornithine Aminotransferase

Sida Shen,[▽] Arseniy Butrin,[▽] Peter F. Doubleday, Rafael D. Melani, Brett A. Beaupre, Mauricio T. Tavares, Glaucio M. Ferreira, Neil L. Kelleher, Graham R. Moran, Dali Liu,* and Richard B. Silverman*

Cite This: *J. Am. Chem. Soc.* 2021, 143, 8689–8703
Read Online
ACCESS | Metrics & More | Article Recommendations | Supporting Information

ABSTRACT: The inhibition of human ornithine δ-aminotransferase (*h*OAT) is a potential therapeutic approach to treat hepatocellular carcinoma. In this work, (*S*)-3-amino-4,4-difluorocyclopent-1-enecarboxylic acid (SS-1-148, **6**) was identified as a potent mechanism-based inactivator of *h*OAT while showing excellent selectivity over other related aminotransferases (e.g., GABA-AT). An integrated mechanistic study was performed to investigate the turnover and inactivation mechanisms of **6**. A monofluorinated ketone (**M10**) was identified as the primary metabolite of **6** in *h*OAT. By soaking *h*OAT holoenzyme crystals with **6**, a precursor to **M10** was successfully captured. This *gem*-diamine intermediate, covalently bound to Lys292, observed for the first time in *h*OAT/ligand crystals, validates the turnover mechanism proposed for **6**. Co-crystallization yielded *h*OAT in complex with **6** and revealed a novel noncovalent inactivation mechanism in *h*OAT. Native protein mass spectrometry was utilized for the first time in a study of an aminotransferase inactivator to validate the noncovalent interactions between the ligand and the enzyme; a covalently bonded complex was also identified as a minor form observed in the denaturing intact protein mass spectrum. Spectral and stopped-flow kinetic experiments supported a lysine-assisted E2 fluoride ion elimination, which has never been observed experimentally in other studies of related aminotransferase inactivators. This elimination generated the second external aldimine directly from the initial external aldimine, rather than the typical E1cB elimination mechanism, forming a quinonoid transient state between the two external aldimines. The use of native protein mass spectrometry, X-ray crystallography employing both soaking and co-crystallization methods, and stopped-flow kinetics allowed for the detailed elucidation of unusual turnover and inactivation pathways.

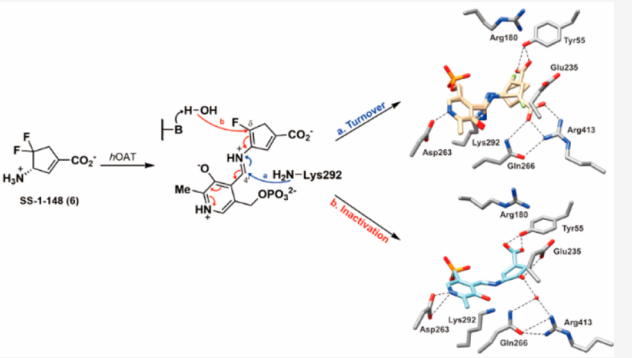

INTRODUCTION

Human ornithine δ-aminotransferase (*h*OAT; EC2.6.1.13) is a pyridoxal-5′-phosphate (PLP)-dependent enzyme that catalyzes two coupled half-reactions, converting L-ornithine (L-Orn) in the first half-reaction to L-glutamate-γ-semialdehyde (L-GSA) and generating L-glutamate (L-Glu) from α-ketoglutarate (α-KG) in the second half-reaction (Figure 1A).[1] The product, L-GSA, is in equilibrium with Δ1-pyrroline-5-carboxylate (P5C), which is converted to L-proline by P5C reductases (PYCRs).[2] The generated L-Glu can also be converted to P5C by pyrroline-5-carboxylate synthase (P5CS), therefore also participating in proline metabolism (Figure 1A).[2] Proline biosynthesis was identified as the most substantially altered amino acid metabolism in human tumor tissues of hepatocellular carcinoma (HCC), featured by accelerated proline consumption, hydroxyproline accumulation, and increased α-fetoprotein (AFP) levels, which are correlated with poor prognosis in HCC.[3] In addition, glutamine synthetase (GS) catalyzes L-Glu's conversion to L-glutamine (L-Gln).[4] L-Gln is required by cancer cells to support the abnormally elevated anabolic processes, thus promoting cellular proliferation.

HCC is the predominant liver malignancy and ranks among the most common causes of cancer-associated mortality worldwide.[5] Our prior DNA microarray analyses identified the *OAT* gene as one of seven overexpressed genes in the spontaneous HCC-developing livers from *Psammomys obesus*

Received: March 4, 2021
Published: June 7, 2021

https://doi.org/10.1021/jacs.1c02456
J. Am. Chem. Soc. 2021, 143, 8689–8703

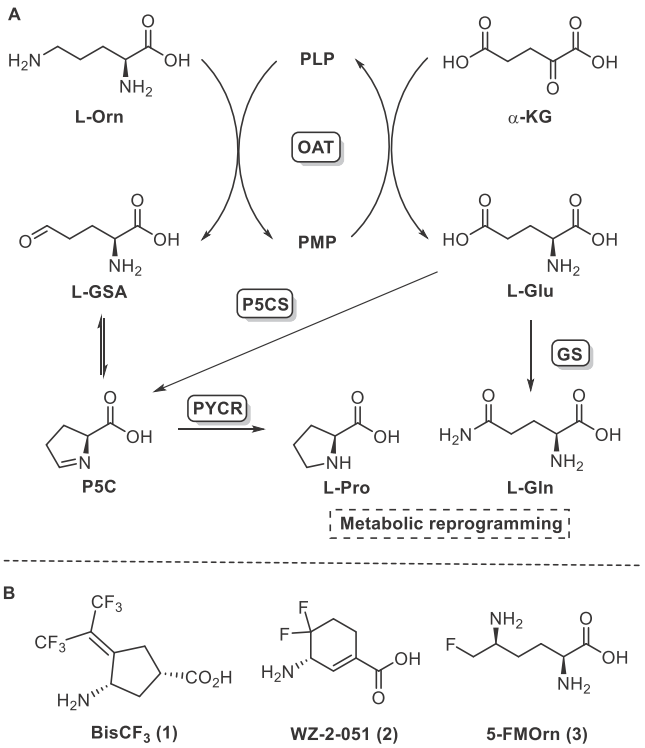

Figure 1. (A) Transamination reactions of *h*OAT and related metabolic pathways. (B) Structures of *h*OAT mechanism-based inactivators **1**−**3**.

(sand rat).[6] Moreover, the treatment (at 0.1 and 1.0 mg/kg; po) of selective *h*OAT mechanism-based inactivator (MBI) $BisCF_3$ (**1**) remarkably decreased the serum AFP levels and inhibited tumor growth in a human-derived HCC mouse model,[6] underscoring the antitumor effects of selective *h*OAT inhibition. A MBI is a molecule that initially acts as an alternative substrate for the target enzyme and is converted by this enzyme to a species that inactivates that enzyme.[7−9] MBIs are typically unreactive before the initial binding with the active site of the target enzyme and usually exhibit significant target specificity and selectivity.[10] Overall, *h*OAT is a potential therapeutic target for HCC, and selectively inactivating *h*OAT may provide a novel opportunity to discover an effective HCC treatment.

The optimization of reversible inhibitors mainly focuses on improving the binding affinity (K_i) or IC_{50} values. In contrast, k_{inact} and K_I values are two critical kinetic parameters for the development of MBIs.[11] The k_{inact} value is the maximal rate constant for enzyme inactivation. The K_I value, the concentration of inactivator that gives the half-maximal inactivation rate, is the inhibition constant, which represents the ability of an MBI to initially bind to the active site of the target enzyme and compete with the substrate. The ratio k_{inact}/K_I is used to evaluate the inactivation efficiency of MBIs.[11]

A major challenge for discovering a selective MBI of *h*OAT is to overcome the irreversible inhibition of other aminotransferases,[7] especially γ-aminobutyric acid aminotransferase (GABA-AT), which has a high structural similarity with *h*OAT.[1] There are only two significant differences in the active site pocket of their homodimer structures: Tyr85 and Tyr55 in *h*OAT are replaced by Ile72 and Phe351* (asterisk denotes arising from the adjacent subunit) in GABA-AT, respectively (Figure 2).[1] Moreover, Ile72 and Phe351* are responsible for the slightly narrower and more hydrophobic active site of GABA-AT relative to *h*OAT. In contrast, the hydroxyl group of Tyr55 serves as a hydrogen bond acceptor to interact with the charged C-2 amino group of substrates, while Tyr85 is a significant determinant of substrate specificity and conformational flexibility to adopt bulky substrates.[1]

Because of the high similarity between these two aminotransferases, a preliminary screening against *h*OAT was carried out previously using our stock GABA-AT inhibitors.[6] A cyclopentane-based analogue, termed $BisCF_3$ (**1**, Figure 1B), bearing a bis(trifluoromethyl) group as its warhead, was identified to be a selective MBI of *h*OAT while only showing millimolar reversible inhibition of GABA-AT. Recent mechanistic studies have revealed that one of its trifluoromethyl groups undergoes fluoride ion elimination, leading the ligand to covalently modify the catalytic Lys292 residue by conjugate addition (Scheme 1 A).[9,12] It is considered that the sterically bulky bis(trifluoromethyl) group may not access the more narrow pocket of GABA-AT as readily, influencing the initial binding pose between the ligand and the enzyme, which may be responsible for its reversible inhibition of this enzyme. Compound **1** has been demonstrated to be effective *in vivo*[6] and is being investigated further in HCC patient-derived xenograft (PDX) models. On the basis of a similar strategy, we enlarged the ring system and further developed a cyclohexene-

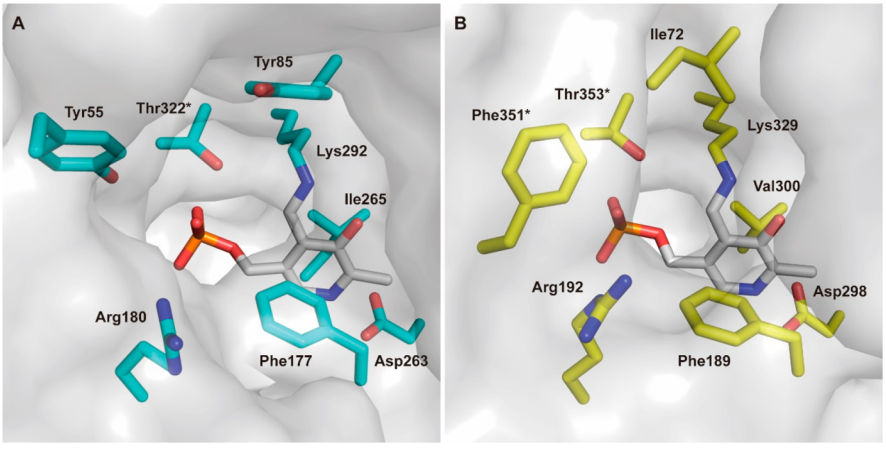

Figure 2. Active site comparison of (A) *h*OAT (PDB entry 1OAT) and (B) GABA-AT (PDB entry 1OHV).

https://doi.org/10.1021/jacs.1c02456
J. Am. Chem. Soc. 2021, 143, 8689−8703

Scheme 1. Inactivation Mechanisms of *h*OAT by 1−3

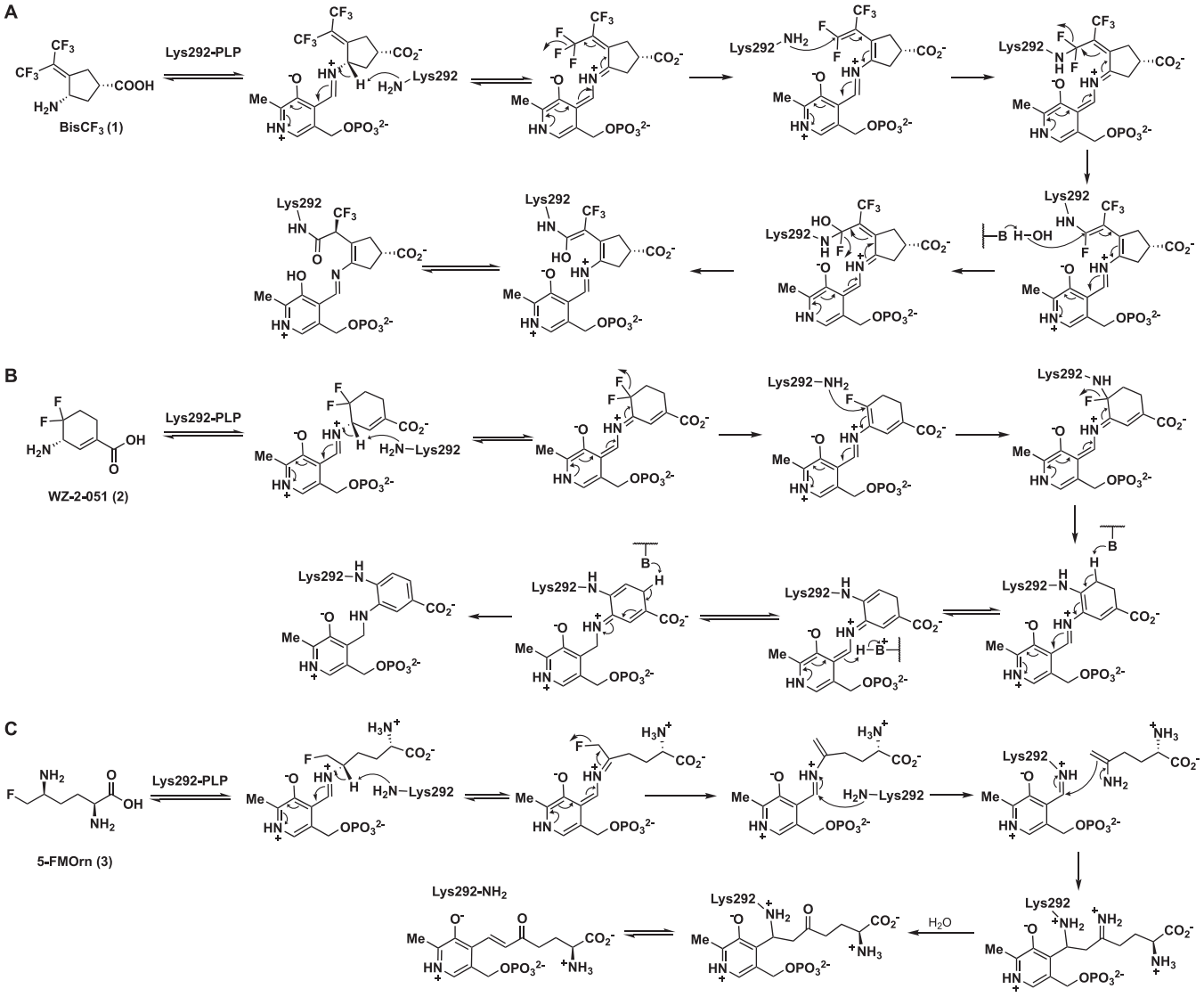

based analogue, WZ-2-051 (**2**, Figure 1B), bearing a difluoro group.[13] Compound **2** exhibited a 23-fold improvement in inactivation efficiency (defined by the k_{inact}/K_I ratio) against *h*OAT compared to **1** while showing 13.3-fold selectivity over GABA-AT. The subsequent mechanistic studies disclosed that **2** undergoes a two-step fluoride ion elimination and inactivates *h*OAT through an addition-aromatization mechanism (Scheme 1 B).[13] An additional example of a selective *h*OAT inactivator is 5-fluoromethylornithine (5-FMOrn, **3**) inspired by the structure of *h*OAT substrate L-Orn and related to the structure of nonselective GABA-AT inactivator (*S*)-4-amino-5-fluoropentanoic acid (AFPA).[14] This molecule inactivates *h*OAT *via* an enamine pathway by forming a ternary adduct (Scheme 1C).[15]

It should be noted that the α-amino group of 5-FMOrn forms a strong hydrogen bond with the phenol group of Tyr55 in the *h*OAT crystal complex (PDB entry 2OAT).[16] Moreover, we also observed hydrogen bonds between the carboxylate groups of **1** (PDB entry 6OIA) and **2** (PDB entry 6V8C) and Tyr55 in *h*OAT crystal complexes.[12,13] Among the published *h*OAT inactivators, only **1** demonstrates (a) promising *h*OAT selectivity through potent irreversible inhibition of *h*OAT, (b) weak, reversible inhibition of GABA-AT (K_i = 4.2 mM), and (c) no inhibition of either aspartate aminotransferase (Asp-AT) or alanine aminotransferase (Ala-AT) (up to 4 mM).[6]

In 2000, (1*R*,4*S*)-4-amino-3,3-difluorocyclopentanecarboxylic acid (**4**, Figure 3) was found to be a reversible inhibitor against GABA-AT (K_i = 0.19 mM).[17] Fifteen years later, it was further demonstrated to be an *h*OAT inactivator.[6] However, **4** exhibits poor binding affinity (K_I = 7.8 mM) and has a low maximum rate of inactivation (k_{inact} = 0.02 min^{-1}) against *h*OAT, only yielding a modest inactivation efficiency (k_{inact}/K_I = 0.003 min^{-1} mM^{-1}).

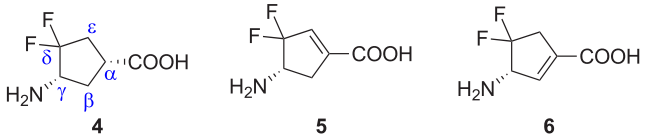

Figure 3. Structures of *h*OAT inactivators **4**−**6**.

In this work, we developed a novel cyclopentene-based analogue **6** by incorporating an additional double bond into the cyclopentane ring system of **4**, which was demonstrated to

https://doi.org/10.1021/jacs.1c02456
J. Am. Chem. Soc. 2021, 143, 8689−8703

Scheme 2. Synthetic Route to 4 and 5[a]

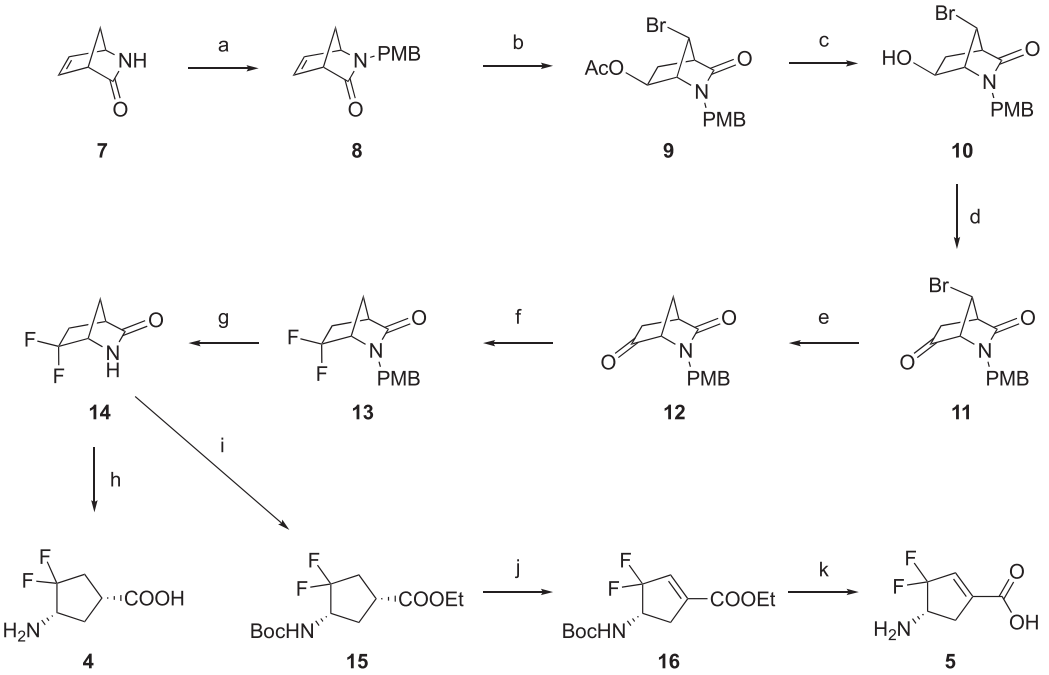

[a]Reagents and conditions. (a) (i) *p*-anisyl alcohol, conc. HCl, rt; (ii) NaH, tetra-*n*-butylammonium iodide (TBAI), THF/DMF (10:1), 0 °C−rt; (b) 1,3-dibromo-5,5-dimethylhydantoin (DBDMH), Ac_2O, rt; (c) K_2CO_3, MeOH/H_2O, rt; (d) $(COCl)_2$, DMSO, TEA, THF, −78 °C−rt; (e) Bu_3SnH, azobis(isobutyronitrile) (AIBN), benzene, reflux; (f) Deoxo-Fluor (2.7 M in toluene), THF, 120 °C (MW); (g) ceric ammonium nitrate, CH_3CN/H_2O, rt; (h) 4 N HCl, AcOH, 70 °C; (i) (i) HCl in EtOH (1.2 M), 70 °C; (ii) Boc_2O, TEA, DCM, rt; (j) PhSeCl, KHMDS (3.0 equiv., 0.5 M in toluene), −78 °C−rt; (k) 4 N HCl, AcOH, 70 °C.

Scheme 3. Synthetic Route to 6[a]

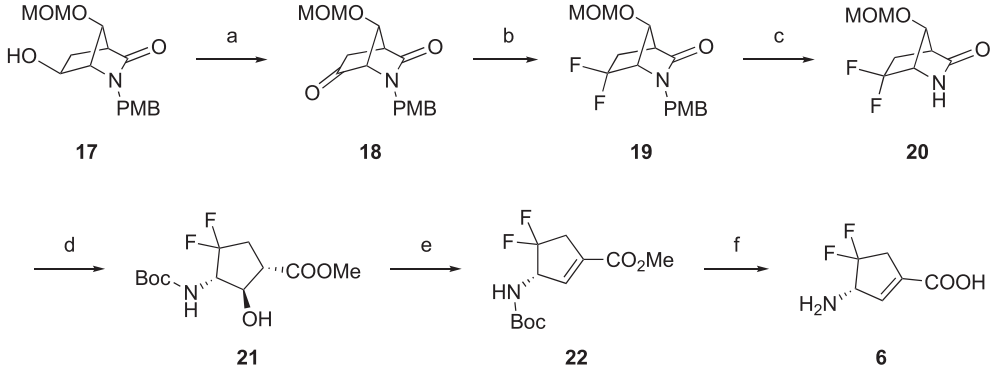

[a]Reagents and conditions. (a) $(COCl)_2$, DMSO, TEA, THF, −78 °C−rt; (b) Deoxo-Fluor (2.7 M in toluene), THF, 120 °C (MW); (c) ceric ammonium nitrate, CH_3CN/H_2O, rt; (d) (i) HCl (1.2 M in MeOH), 85 °C, seal; (ii) Boc_2O, MeOH, rt; (e) Burgess reagent, THF, 70 °C; (f) 4 N HCl, AcOH, 70 °C.

be a potent and selective *h*OAT inactivator. Furthermore, we performed mechanistic studies utilizing protein crystallography, multiple modes of mass spectrometry, transient-state spectrophotometric measurements, and computational simulations to reveal a novel noncovalent inactivation mechanism for **6**.

RESULTS AND DISCUSSION

Synthesis of Cyclopentene Analogues 5 and 6 Bearing a *gem*-Difluoro Group. On the basis of our previous experience with the discovery of GABA-AT inactivators, the incorporation of a double bond into a cyclopentane ring has been demonstrated to be an effective strategy for improving inactivation efficiency, which influences the configuration of the initial external aldimine and the adjunct proton's acidity resulting from the α,β-unsaturated carboxylate.[18,19] Therefore, we designed cyclopentene-based analogues **5** and **6** bearing a *gem*-difluoro group on the basis of the structure of parent compound **4** (Figure 3) with the intent to develop more potent *h*OAT inactivators.

The synthetic route to prepare compound **5** initiated from the enantiopure Vince lactam[20] (**7**; (1*R*)-(−)-2-azabicyclo-[2.2.1hept-5-en-3-one; CAS#: 79200-56-9) to afford the key bicyclic intermediate **9** according to the procedure developed previously (Scheme 2).[17] The acetyl group of **9** was then hydrolyzed under acid conditions followed by Swern oxidation, yielding ketone intermediate **11**.

https://doi.org/10.1021/jacs.1c02456
J. Am. Chem. Soc. 2021, 143, 8689−8703

Table 1. Kinetic Constants for the Inactivation of *h*OAT and Reversible Inhibition of GABA-AT by 4−6[a]

Cmpd	Structure	*h*OAT					GABA-AT
		k_{inact} (min^{-1})	K_I (mM)	k_{inact}/K_I ($min^{-1}mM^{-1}$)	Partition ratio[c]	Fluoride ion release (eq.)[d]	K_i (mM)
1	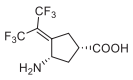	0.09 ± 0.01	0.09 ± 0.03	1.0 ± 0.4	12 ± 1[b]	79 ± 2[b]	5.2 ± 0.6
4	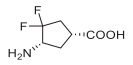	0.01 ± 0.00	4.00 ± 1.00	0.003 ± 0.001	2200 ± 70	3400 ± 30	0.1 ± 0.0
5	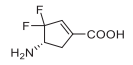	0.03 ± 0.01	2.00 ± 0.90	0.015 ± 0.006	790 ± 35	750 ± 60	1.4 ± 0.1
6	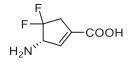	0.08 ± 0.01	0.06 ± 0.03	1.3 ± 0.7	34 ± 0	34 ± 1	1.1 ± 0.1

[a] k_{inact} and K_I values were determined by the equation: $k_{obs} = k_{inact} \times [I]/(K_I + [I])$ and presented as means and standard errors. K_i values were calculated by the Cheng-Prusoff equation: $K_i = IC_{50}/(1 + [S]/K_m)$ and shown as means and standard errors. IC_{50} values were obtained using nonlinear regression analysis in GraphPad Prism 8 of a 9-point enzymatic assay with a 2-fold serial dilution against GABA-AT. The partition ratios were determined under conditions in the presence of α-KG, while fluoride ion release results were determined in the absence of α-KG. [b]Data were extracted from ref 12. [c]Enzyme activity remaining was measured as a function of the number of equivalents of **4**−**6** relative to enzyme concentration. Linear regression analysis was used on the linear portion of the curves to obtain the x-intercept, which was the turnover number (partition ratio = turnover number − 1). Data are shown as the means with standard errors. [d]The fluoride ion release experiments were performed in triplicate. Data are presented as the means with standard deviations.

Subsequently, the reduction of the bromo group on the bridgehead of **11** to form **12** was carried out with Bu_3SnH/AIBN by a published procedure.[17] Intermediate **12** was treated with Deoxo-Fluor reagent under microwave conditions to afford difluoro intermediate **13**. The PMB protecting group of **13** was removed using ceric ammonium nitrate (CAM) to produce lactam **14.** The treatment of **14** with HCl/EtOH under reflux conditions followed by Boc protection yielded **15**. Unexpectantly, when we attempted to selenate **15** at the α-position of the ethyl ester with KHMDS (3.0 equiv) and PhSeCl for the follow-up α-elimination reaction,[18] intermediate **16**, bearing an α,ε-conjugated carboxylate group, was produced directly as the sole product. Because of the strong electron-withdrawing effect of the *gem*-difluorines, the theoretical pK_a values of the hydrogens at the C_ε position are considerably decreased, which are further decreased by the incorporation of the phenylselenyl group (Scheme S1). This should facilitate deprotonation in the presence of excess KHMDS, thereby causing the elimination of the phenylselenyl group. 1D and 2D NMR spectra were obtained to validate the structure of **16**. Cyclopentene-based analogue **5** was generated after deprotection under acidic conditions. The parent cyclopentane-based analogue (**4**) was also prepared from intermediate **14** by acid hydrolysis and was evaluated together with new analogues and **1** in subsequent kinetic studies.

The synthetic route to **6** started from the preparation of the critical bicyclic intermediate **17** from PMB-protected Vince lactam **8** following our recently published procedure (Scheme 3).[19] The hydroxyl group of **17** was converted to ketone **18** by Swern oxidation. Difluoro intermediate **19** was obtained through the same fluorination conditions described in Scheme 2. The PMB group of **19** was removed by ceric ammonium nitrate followed by lactam hydrolysis and Boc protection, yielding cyclopentane intermediate **21**. The hydroxyl group of **21** was dehydrated using Burgess reagent[21,22] under reflux, forming cyclopentene intermediate **22**. The final product (**6**) was afforded using the deprotection conditions in Scheme 2.

Kinetic Studies of Analogues 4−6. The kinetic results in Table 1 indicate that all three difluoro-based compounds **4**−**6** are irreversible inhibitors of *h*OAT but reversible inhibitors of GABA-AT. Whereas inactivators **4** and **5** are weak binding inactivators (K_I = 4.0 and 2.0 mM, respectively) of *h*OAT, **6** exhibited a significantly higher affinity (K_I = 0.06 mM). The partition ratio is defined as the ratio of the number of equivalents of inactivator consumed as a substrate per active site compared to each equivalent of inactivator leading to inactivation.[18,23] The fluoride ion release result is determined as the equivalents of fluoride ions released per active site for each inactivation event, which can be measured with a fluoride ion-selective electrode.[23] The partition ratio determination and fluoride ion release results in Table 1 revealed that the majority of reactions of **4** and **5** involve an alternative turnover pathway, resulting in the release of a large fraction of fluoride ions. Compound **6** showed the highest maximal rate constant of inactivation (k_{inact}) relative to **4** and **5**, thereby leading to superior inactivation efficiency (k_{inact}/K_I) (**4** vs **6**, 0.003 vs 1.300 min^{-1} mM^{-1}, a 400-fold improvement). Furthermore, the inhibitory activities of cyclopentene-based **5** (K_i = 1.40 mM) and **6** (K_i = 1.10 mM) toward GABA-AT are about 10-times weaker than that of cyclopentane-based **4** (K_I = 0.10 mM). It should be noted that, compared to parent cyclopentane **4** (OAT, K_I = 4 mM; GABA-AT, K_I = 0.10 mM), newly developed cyclopentene **6** displayed a significantly higher binding affinity for OAT but much lower binding affinity for GABA-AT (OAT, K_I = 0.06 mM; GABA-AT, K_i = 1.10 mM), indicating **6** has an improved ability to more

https://doi.org/10.1021/jacs.1c02456
J. Am. Chem. Soc. 2021, 143, 8689−8703

Scheme 4. Possible Inactivation Mechanisms for 6

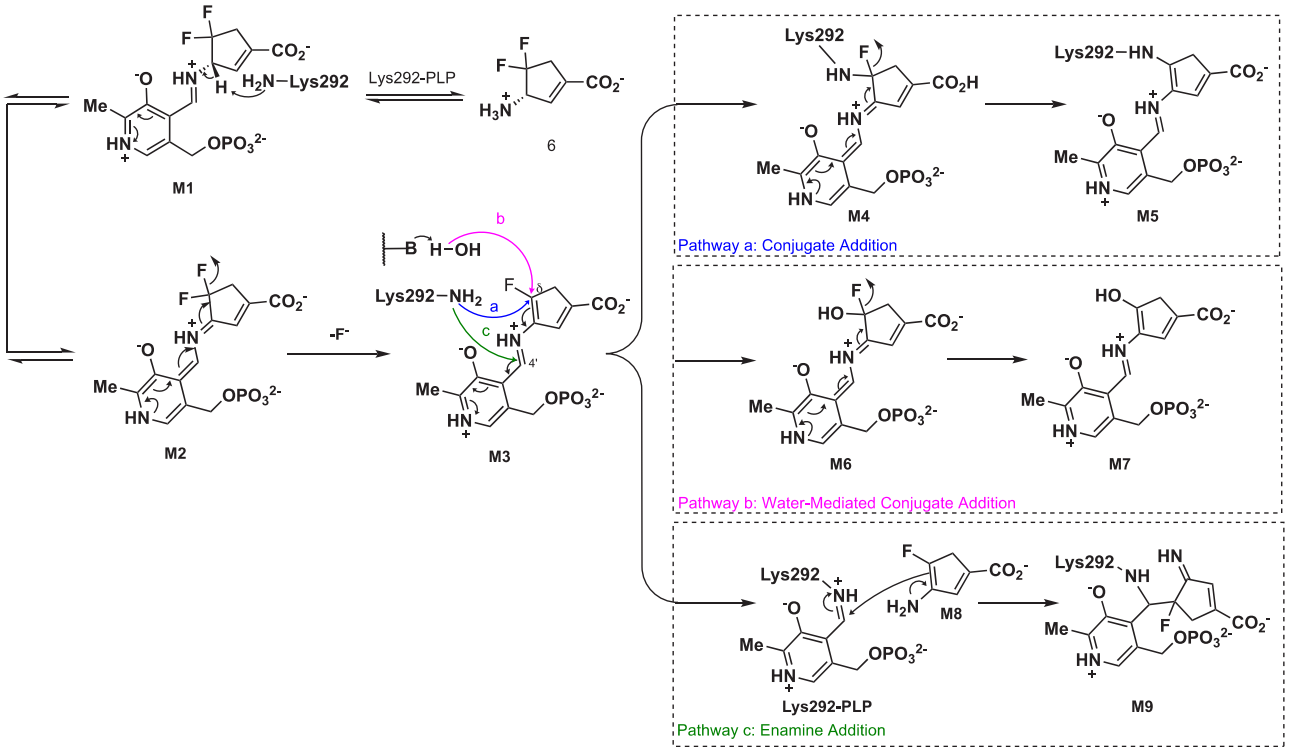

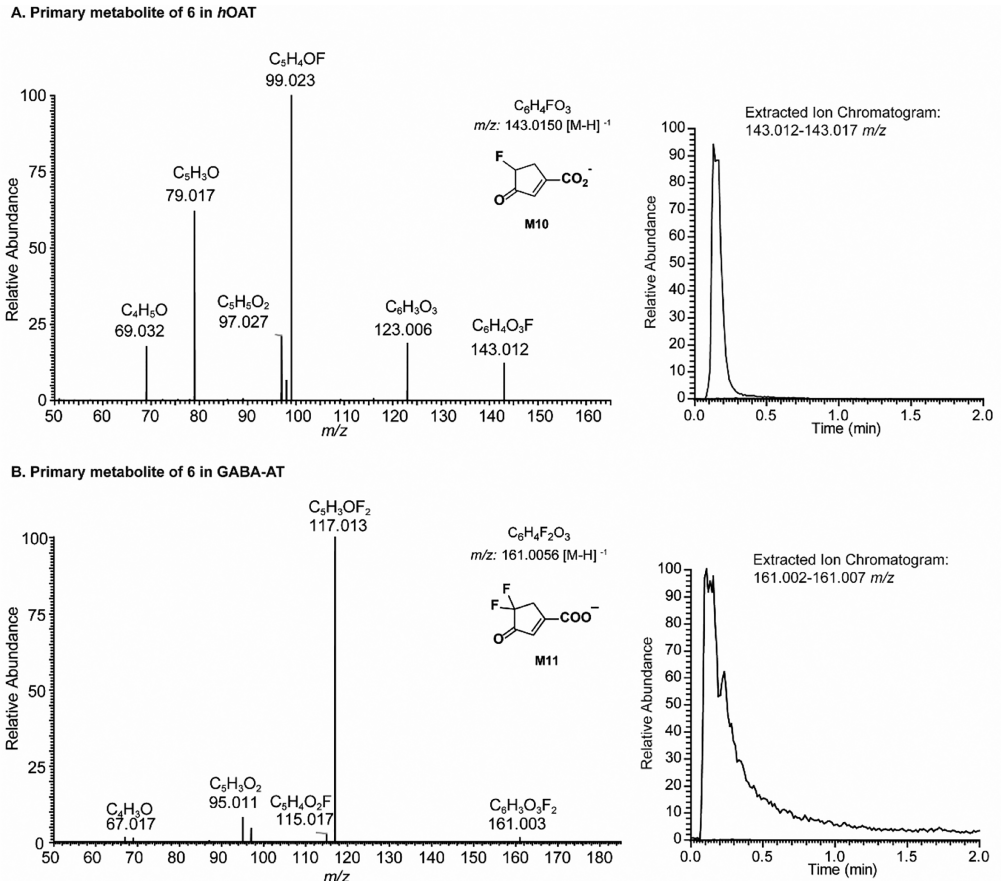

Figure 4. Primary metabolites of **6** in (A) *h*OAT and (B) GABA-AT.

selectively bind with OAT relative to GABA-AT. Compound **6**, also called SS-1-148, exhibited comparable inactivation efficiency against *h*OAT while retaining the reversible inhibition of GABA-AT similar to that of the preclinical

https://doi.org/10.1021/jacs.1c02456
J. Am. Chem. Soc. 2021, 143, 8689−8703

Scheme 5. Plausible Turnover Mechanisms of 6 with *h*OAT and GABA-AT

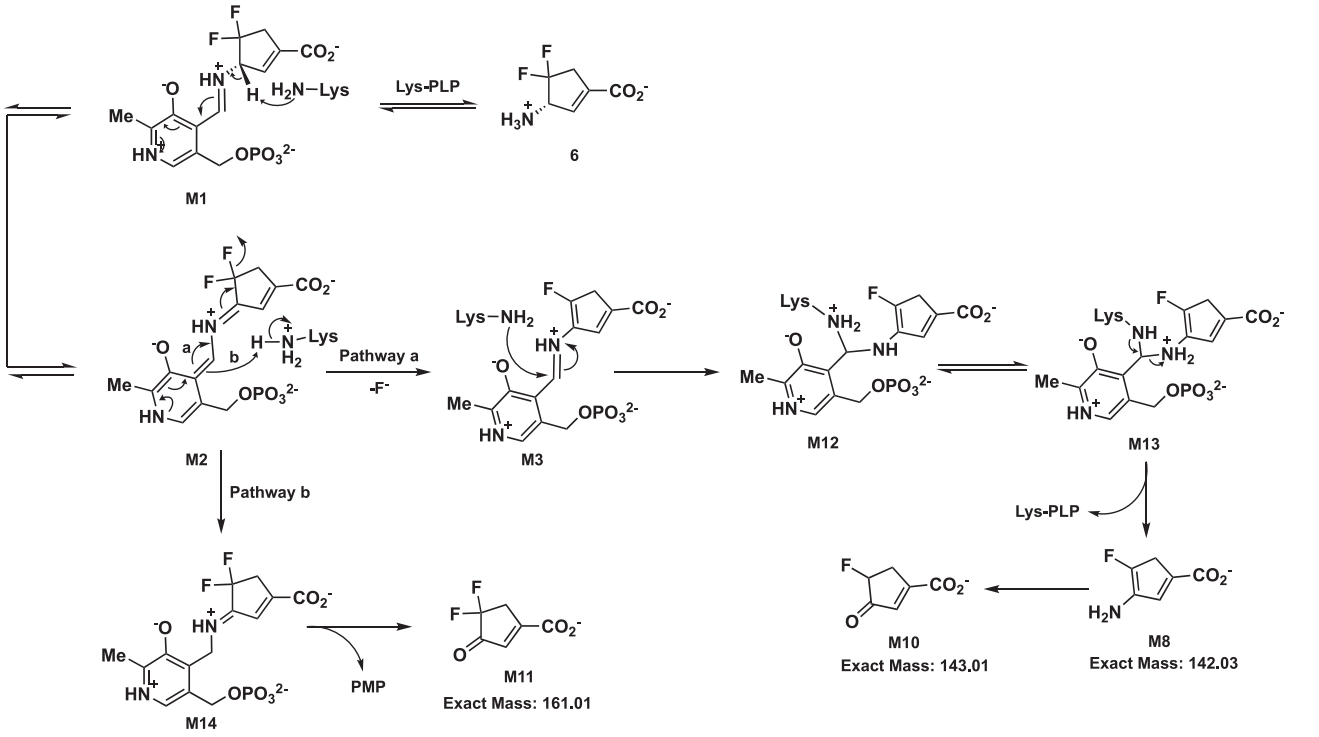

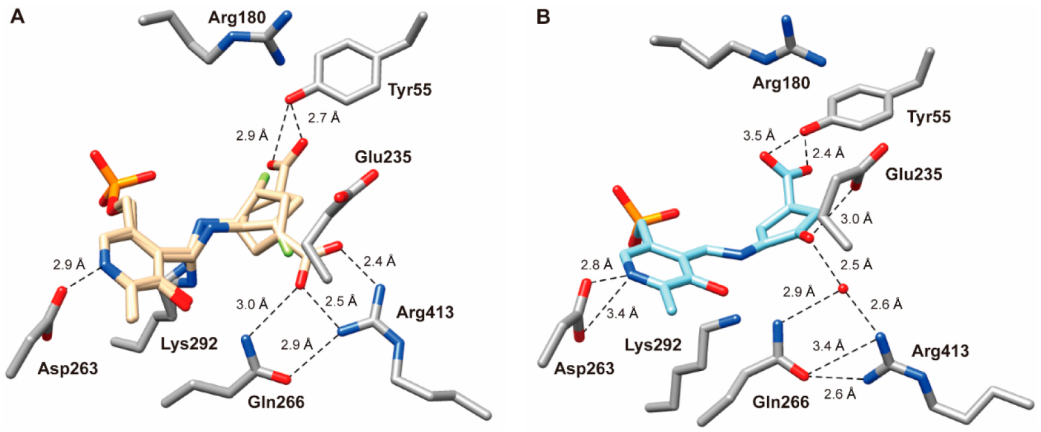

Figure 5. Crystal structures of *h*OAT resulting from the (A) soaking experiment (PDB entry 7LK1) and (B) co-crystallization (PDB entry 7LK0) with **6**. The **6** soaking structure is shown in two alternate conformations (beige): one in which the carboxylate group interacts with Tyr55 (conformation A) and the other in which the carboxylate forms a salt bridge with Arg413 (conformation B). For this specific chain, the refined occupancies of conformers are 0.51 (conformation A) and 0.49 (conformation B). *h*OAT residues are in stick representation with carbon atoms in the residues colored gray, nitrogen in blue, and oxygen in red; the water molecule is shown as a red sphere. Hydrogen bonding distances between atoms are in Ångstroms (Å) and are shown as black dashed lines.

compound **1**. It also did not show a noticeable inhibition of Asp-AT or Ala-AT at concentrations up to 10 mM, motivating interest in the elucidation of the inactivation and turnover mechanisms of **6** with *h*OAT.

Proposed Inactivation Mechanism Pathways of 6. On the basis of our previous mechanistic studies of other related GABA-AT/*h*OAT inactivators,[8,13] we propose three potential pathways (Scheme 4). Initially, transimination with **6** would form the external aldimine **M1**. **M1** would then undergo deprotonation to form the quinonoid species **M2** followed by fluoride ion elimination, affording the intermediate (**M3**) that can branch into three different pathways.

Pathway a is proposed on the basis of our recent findings with the cyclohexene-based analogue **2**.[13] The electrophilic C_δ position of intermediate **M3** could undergo conjugate addition by Lys292, forming a covalent bond (**M4**). Quinonoid species **M4** is also subject to a second fluoride ion elimination to give final adduct **M5**. *Pathway b* is inspired by the inactivation mechanisms of CPP-115[23] and OV329[18] with GABA-AT, which are achieved through a water-mediated mechanism, resulting in tight electrostatic interactions between their carboxylates and arginine residues in the active site. Lys292 would then activate a water molecule that attacks the electrophilic C_δ position of intermediate **M3** followed by a further fluoride ion elimination that would yield enol/carbonyl

https://doi.org/10.1021/jacs.1c02456
J. Am. Chem. Soc. 2021, 143, 8689−8703

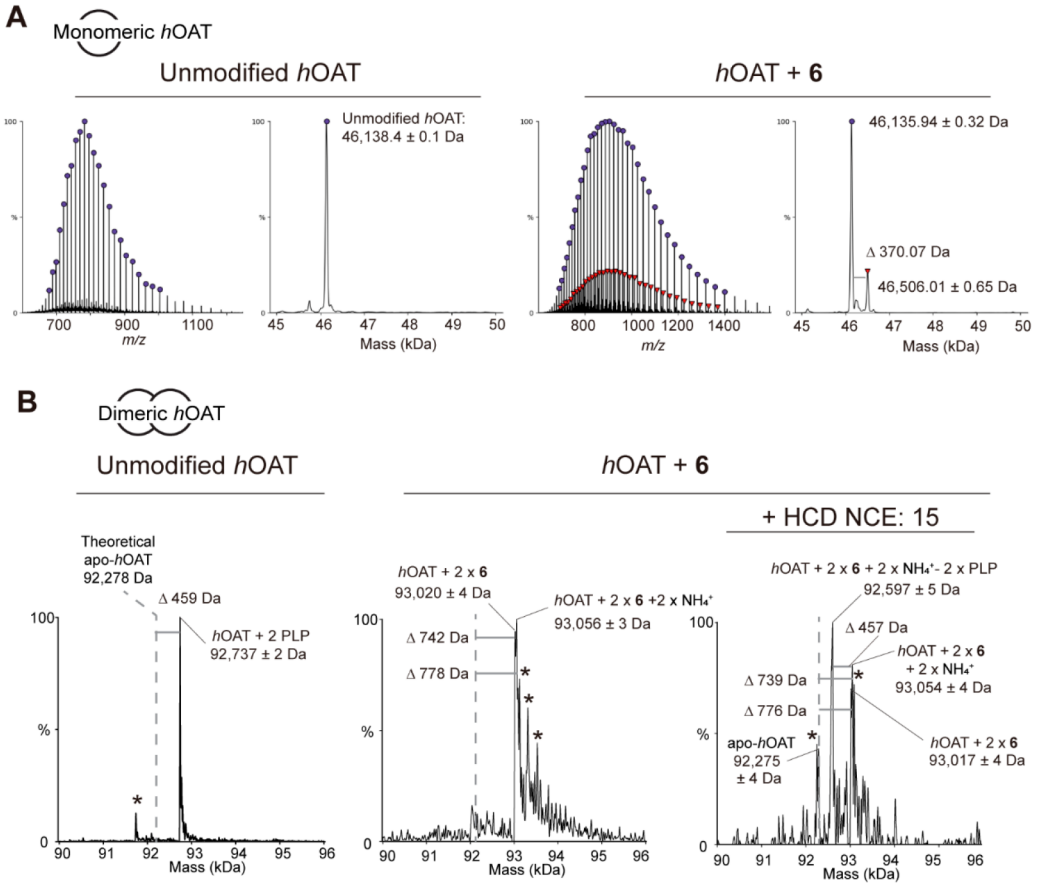

Figure 6. (A) Denaturing and (B) native intact protein mass spectrometry of *h*OAT untreated and inactivated by **6**.

species **M7** rather than establishing a covalent bond with the catalytic lysine residue in *h*OAT. *Pathway c* is proposed according to a typical enamine mechanism.[19] Lys292 attacks the $C_{4'}$ position of the aldimine instead of the C_{δ} position while releasing enamine intermediate **M8**, which attacks the imine linkage of the internal aldimine (PLP-Lys292) and produces covalent adduct **M9**.

Plausible Turnover Mechanisms of 6 with *h*OAT and GABA-AT. Compound **6** exhibited a relatively high partition ratio (34-fold, Table 1 and Figure S1), indicating that 35 equiv of **6** are turned over per active site for each equivalent of compound leading to inactivation. Moreover, 34 ± 1 equiv of fluoride ion (Table 1) are released per inactivation event, indicating that the primary turnover pathway only involves a single fluoride ion elimination step. Previously, we carried out electrostatic potential (ESP) charge calculations to demonstrate that the fluorine atom decreases the nucleophilicity of the enamine intermediate (similar to the structure of **M8**),[13] which may prevent enamine addition. A mass spectrometry (MS)-based analysis of **6** with *h*OAT (Figure 4A) showed that the molecular weight and fragmentations of the primary metabolite match the structure of **M10** in Scheme 5, the hydrolyzed product of enamine intermediate **M8**. Conversely, we also identified the primary metabolite of **6** in GABA-AT (Figure 4B). The molecular weight and fragmentations suggest that **6** acts as a substrate with this enzyme to yield ketone **M11**, bearing a difluoro group (Scheme 5).

In an attempt to capture the primary intermediate of the noninactivation pathway, *h*OAT holoenzyme crystals were utilized to perform one-hour soaking experiments with **6**. The *h*OAT structure was solved by molecular replacement from a previously reported structure (PDB entry 1OAT). The space group for the **6** soaking structure was found to be $P3_221$, and the structure contains three copies of the protein monomer in one asymmetric unit. The crystal structure (PDB entry 7LK1) shown in Figure 5A and Figure S3 indicates that PLP is covalently linked to **6**, and a covalent bond between Lys292 and **6** tethers the compound to the enzyme. The covalent bond between Lys292 and **6** represents a stable *gem*-diamine species that has not been observed in any previous *h*OAT/ligand crystals.[9,12,13,24] This observation further validated the *gem*-diamine precursors (**M12** or **M13**, Scheme 5) of enamine intermediate **M8**. Moreover, two alternate conformations of this intermediate were observed, which differ in the position of the carboxylate group derived from **6**. The first conformation forms a hydrogen bond between Tyr55 and the carboxylate of **6**, while the second forms a salt bridge with Arg413. The interpretation that there are two alternate conformations for the intermediate structure was based on the positive density in proximity to Arg413 and Tyr55 as well as the relatively high B-factors for any single conformation. An alternative explanation could include two different, yet structurally similar, intermediate species that could interact with the protein active site in different ways.

The dominant turnover mechanisms for **6** in *h*OAT and GABA-AT are proposed in Scheme 5. After capturing the PLP coenzyme from Lys292, **M1** undergoes deprotonation to give quinonoid **M2** that causes the elimination of a fluoride ion (*Pathway a*; Scheme 5) in *h*OAT to produce aldimine **M3** bearing a single fluorine atom. The majority of **M3** is attacked

https://doi.org/10.1021/jacs.1c02456
J. Am. Chem. Soc. 2021, 143, 8689−8703

Scheme 6. Possible Inactivation Mechanisms of 6 with *h*OAT

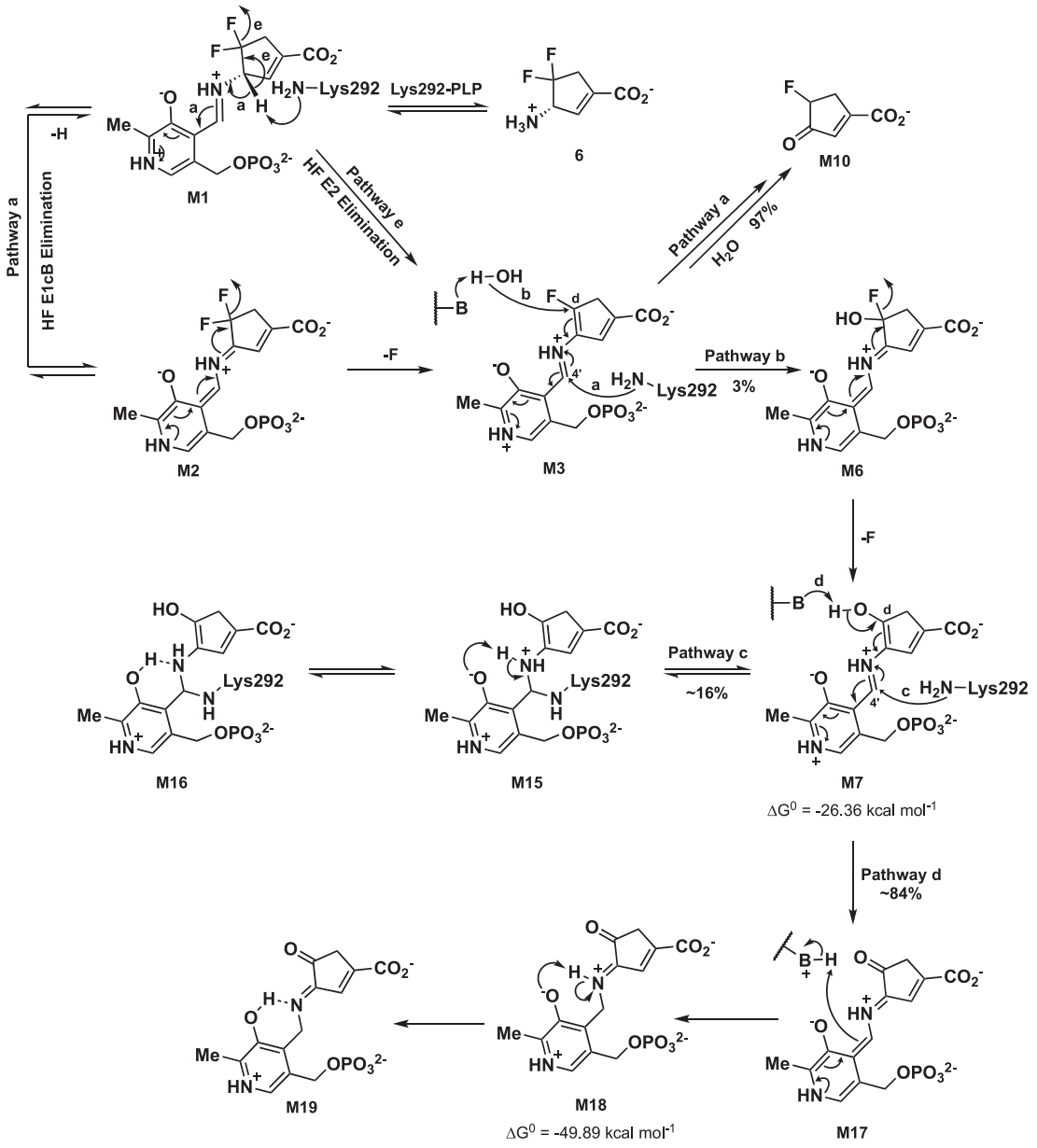

by Lys292 at its $C_{4'}$ position, forming the first *gem*-diamine (**M12**), followed by proton transfer,[25,26] which results in the second *gem*-diamine (**M13**), which is further converted to enamine metabolite **M8** and the internal aldimine. **M8** undergoes hydrolysis to ketone **M10** as the primary metabolite of **6** in *h*OAT. In contrast, quinonoid intermediate **M2** only undergoes electron transfer to yield ketimine **M14**, which hydrolyzes to release PMP and **M11** as the primary metabolites in the GABA-AT reaction. The behavior of **6** in GABA-AT mimics a canonical transamination reaction without eliminating fluoride ions, consistent with its reversible inhibition of GABA-AT. Given the structural differences between *h*OAT and GABA-AT, the known selective *h*OAT inactivators (**1**−**3**) described above contain a bulky moiety or α-amino group to improve their selectivity. However, the selectivity of **6** for *h*OAT over GABA-AT occurs because of its competition with substrate GABA.

Plausible Inactivation Mechanisms of 6 with *h*OAT. The irreversibility of the inhibition of *h*OAT by **6** was evaluated with a 48 h time-dependent dialysis experiment against a buffer containing excess PLP and α-KG (Figure S2). The residual activity of *h*OAT was unchanged, demonstrating that **6** is an irreversible inhibitor of this enzyme. To reveal the structure of the final product of the inactivation reaction, we co-crystallized *h*OAT in the presence of excess **6**. The crystal structure (PDB entry 7LK0) was solved using the same procedure described above. The space group for the **6** co-crystal (Figure 5B and Figure S4) was found to be $P3_112$ and contained three subunits per asymmetric unit. Similar to the soaking crystal structure shown in Figure 5A and Figure S3, PLP is covalently linked to the **6** moiety in the co-crystal structure. However, no covalent bond is observed between Lys292 and the final product. Moreover, in the published crystal structure of the native enzyme (holo-*h*OAT; PDB entry 1OAT), Arg413 typically forms a salt bridge with Glu235, which was observed for several co-crystals of *h*OAT with different inactivators.[16,24,27] In the *h*OAT/**6** soaking structure (Figure 5A), the salt bridge of Arg413-Glu235 is broken

https://doi.org/10.1021/jacs.1c02456
J. Am. Chem. Soc. 2021, 143, 8689−8703

because of the formation of an alternative salt bridge between the carboxylate of one intermediate and Arg413. Interestingly, the Arg413−Glu235 salt bridge is also found to be broken in the *h*OAT/**6** co-crystal structure, while no direct interaction is observed between Arg413 and the ligand. Instead, Arg413, Gln266, and the final product are hydrogen-bonded to the same water molecule. Additionally, the carbonyl oxygen of the ligand shows a hydrogen bond with Glu235 (3.0 Å) (Figure 5B), which may contribute to stabilizing the ligand in the *h*OAT pocket. The ligand structure in the *h*OAT/**6** co-crystal structure indicates that the inactivation may be attributed to *Pathway b* in Scheme 4, generating a final product that resembles **M7** (theoretical mass: 370.06 Da).

We previously have applied denaturing intact protein mass spectrometry (denaturing MS) to probe covalent inactivation mechanisms of *h*OAT inactivators.[12,13] Here, through denaturing MS using *h*OAT fully inactivated by **6**, only ∼16% of *h*OAT was found to be covalently modified, leading to a mass increase of 370.07 Da (Figure 6A, right). The majority of *h*OAT remained unmodified (Figure 6A, right) like the untreated *h*OAT used as a control (Figure 6A, left). The observed mass addition (370.07 ± 0.82 Da) corresponds to the theoretical mass of *gem*-diamine **M15** (370.06 Da; Scheme 6) that could be in equilibrium with the noncovalent form **M7**. However, we would expect a higher abundance of the covalently bound enzyme under these conditions where the enzyme is fully inactivated. This finding supports a noncovalent inactivation mechanism between *h*OAT and **6**.

We further employed native mass spectrometry (native MS) to identify solution-state, noncovalent protein interactions that are preserved in the gas phase and characterized the binding of the **6** product in *h*OAT. The results shown in Figure 6B indicate that untreated *h*OAT appears as a dimer (92,737 ± 2 Da) that is 459 Da more than the mass of the apo-*h*OAT dimer. This mass shift is consistent with two PLP-bound internal aldimines that reside in the active sites of the dimer (459 Da shift observed; 460 Da theoretical). A proteolytic proteoform of *h*OAT was also observed, but only under untreated conditions (Figure 6B, left (*)). In contrast, native, dimeric *h*OAT fully inactivated by **6** was observed with two high-abundance masses of 93 020 ± 4 Da and 93 056 ± 3 Da, corresponding to a mass addition of 742 and 778 Da, respectively (Figure 6B, middle). Several additional masses were observed and can be attributed to salt adducts (Figure 6B, middle (*)). In addition, neither unmodified apo-*h*OAT nor PLP-bound *h*OAT was observed. The observed 93,020 ± 4 Da mass is consistent with the predicted mass of **M7** (370.06 Da) bound in both active sites (theoretical: 93 018 Da). As the *h*OAT samples were desalted by dialyzing against 100 mM NH_4OAc solution for 1 week, we think that the 93 056 ± 3 Da observed mass is the predicted mass of **M7** complexed with one ammonium cation ($[M + NH_4]^+$ = 388.09 Da) in both protein chains (theoretical: 93 054 Da).

To further probe the lability of the **6**-*h*OAT interaction by mass spectrometry, higher-energy collisional dissociation (HCD) was applied to untreated and treated *h*OAT to dissociate the protein−ligand interactions and eject ligands from the enzyme complex. To eject adducts from protein dimers, HCD was applied with normalized collisional energy (NCE) ranging from 5 to 15%. No mass shift was observed for untreated *h*OAT (Figure S5). Under these same conditions, two additional masses were produced for **6**-inactivated *h*OAT (Figure 6B, right). One mass, consistent with apo-*h*OAT, was observed at 45% relative abundance (observed: 92 275 ± 4 Da; theoretical: 92 278 Da), and a second mass of 92 597 ± 5 Da was observed at 100% relative abundance. Compared to the previously observed dimer mass, which is consistent with each active site bound by **M7** and one ammonium cation, this species has a 457 Da mass shift. Interestingly, the high abundance mass shift cannot be explained by the loss of a single **M7** ± NH_4^+ adduct from the protein dimer (theoretical mass for **M7**-*h*OAT: 92 648 Da; theoretical mass for **M7**-*h*OAT+ NH_4^+: 92 666 Da). The mass shift observed through HCD activation, however, can be explained by the loss of PLP from both active sites, while the **6** moiety with one ammonium cation was apparently retained (observed: 457 Da; theoretical: 460 Da). This finding is surprising, given that the same collisional energy does not eject PLP from the untreated protein dimer (Figure S5).

As no apoenzyme is observed by native MS and approximately 84% of *h*OAT was in an apoenzyme state under denaturing MS conditions at pH 2.5, these results indicate that noncovalent **M7** is the primary form after inactivation, while covalently bound **M15** is a minor form that is in equilibrium with **M7**. Therefore, **M7** generated from the water-mediated *Pathway b* (Scheme 4) seems to be the final product of **6** after inactivation. However, given its highly conjugated structure, **M7** readily tautomerizes. A Gibb's free energy calculation[28] was performed on MOPAC to assess the stabilities of **M7** and the related tautomeric forms in the *h*OAT's active site. The results shown in Figure S6 suggest that, compared with enol form **M7** (Tautomer 1; ΔG° = −26.36 kcal mol^{-1}), the corresponding ketone (Tautomer 5, ΔG° = −48.07 kcal mol^{-1}) and two potential ketimines (Tautomer 8, ΔG° = −49.89 kcal mol^{-1} and Tautomer 9, ΔG° = −49.07 kcal mol^{-1}) are relatively more stable. Moreover, a species that shows absorbance at ∼275 nm was determined as the final product in the subsequent transient-state spectrophotometric measurements (Figure 8C), thereby ruling out all external aldimines (e.g., **M7** and Tautomer 5) that would display absorbance maxima at ∼420 nm. The results above indicate that the final state is more likely a *gem*-diamine or ketimine that typically has an absorbance maxima ∼330−340 nm.[25,29] According to the literature, in comparison with the ketoenamine moiety, containing a protonated aldimine and deprotonated hydroxyl, the neutral enolimine of the hydroxyl and aldimine groups exhibit shifted the absorption maximum (410 vs 330 nm).[30] Taken together, we believe that *gem*-diamine **M15** (Scheme 6) is in equilibrium with **M7**, and ketimine **M18** is tautomerized from **M7**; both **M15** and **M18** may then undergo additional electron transfer to form **M16** and **M19**, respectively. Because of the neutral states of *gem*-diamine **M16** and ketimine **M19**, their absorption transitions shift from 330 to 275 nm, consistent with the absorbance of the final species observed in the transient-state measurements.

Proposed inactivation pathways for **6** with *h*OAT are summarized in Scheme 6. The initial external aldimine **M1** undergoes deprotonation, catalyzed by Lys292, and forms the first quinonoid (**M2**). The elimination of a single fluoride ion follows to yield monofluoro aldimine **M3** from **M2**. The $C_{4'}$ position of the majority of **M3** (∼97%; determined by its partition ratio) is attacked by Lys292, which releases an enamine metabolite that hydrolyzes to ketone **M10** as the primary metabolite (*Pathway a*; Schemes 5 and 6).

The C_δ position of a small portion of **M3** (∼3%) goes through a water-mediated nucleophilic attack (*Pathway b*;

https://doi.org/10.1021/jacs.1c02456
J. Am. Chem. Soc. 2021, 143, 8689−8703

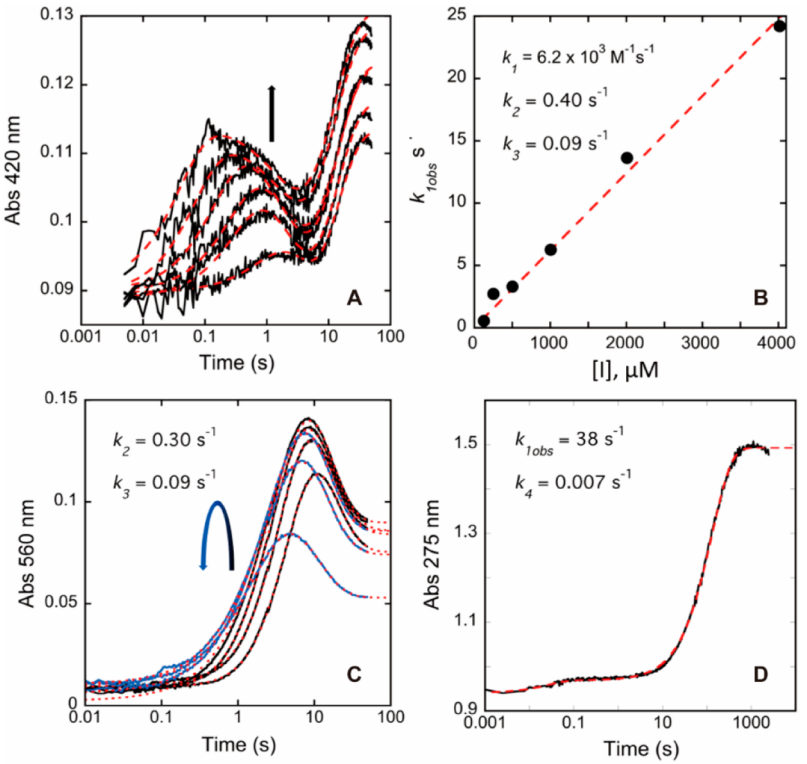

Figure 7. Transient state absorption changes observed at 275, 420, and 560 nm for *h*OAT reacting with **6**. OAT (12.7 μM final) was mixed with **6** (126, 251, 502, 1004, 2008, and 4016 μM), and CCD spectra were collected for the time frame 0.009−49.2 s. (A) Data observed at 420 nm fit to a linear combination of three exponential terms according to eq S3 described in the Supporting Information. The arrow indicates the trend observed in amplitude for increasing inhibitor concentration. (B) Observed rate constant dependence of the first phase observed at 420 nm fits eq S5 described in the Supporting Information. The values for k_2 and k_3 indicated are the average values obtained from the fit in Figure 7A. The fit is shown by red dashes. (C) Data observed at 560 nm. The curved arrow indicates the trend observed in amplitude for increasing inhibitor concentration. These data were fit to a linear combination of two (1004, 2008, and 4016 μM, blue traces) or three (126, 251, and 502 μM, black traces) exponential terms according to eq S4 described in the Supporting Information. The fit is shown by red dashes. (D) Data observed at 275 nm over 2000 s obtained in the presence of 8032 μM **6** fit a linear combination of two exponential terms according to eq S4 in the Supporting Information. The fit is shown by red dashes.

Scheme 6), generating the second quinonoid (**M6**). Intermediate **M6** undergoes another fluoride ion elimination to form **M7**. Subsequently, a small fraction of **M7** (~16%) may covalently bond to Lys292 at its $C_{4'}$ position *via* a *gem*-diamine form (**M15**) (*Pathway c*; Scheme 6), which is in equilibrium with **M7** and also facilitates further proton transfer to generate the neutral *gem*-diamine (**M16**), which should be a more stable form. However, the majority of **M7** (~84%) tautomerizes to a more favorable ketimine (**M18**, the most stable tautomeric form in Figure S6), which is followed by proton transfer to afford ketimine **M19** as the primary final product (*Pathway d*; Scheme 6).

Transient-State Measurements of *h*OAT Inhibited by 6. As a variety of transient states are involved in the proposed mechanisms, we performed rapid-mixing spectrophotometric measurements in an attempt to capture the kinetics of the inhibition of *h*OAT by **6**. This approach takes advantage of the conjugated species that accumulate sequentially in PLP-dependent aminotransferase reactions.[9] The inhibition reaction that occurs with **6** was interpreted in combination with crystal structures (mentioned above) acquired for different stages of the reaction progression. The experimental data shown in Figures 7 and 8 indicate that the reaction of **6** with *h*OAT is complex. Four discernible phases were observed with the evidence of at least two parallel reaction paths (Figure 8), indicating that the mechanistic conclusions drawn are necessarily from undetermined models. Within the deadtime of the stopped-flow instrument, the reaction of **6** with *h*OAT formed a spectrum signal (~420 nm) consistent with an external aldimine (red spectrum, Figure 8A,B). The titration of *h*OAT with **6** modulated the rate and the extent of accumulation of a second external aldimine that is presumably additive with the aldimine formed in the deadtime (green spectrum, Figure 8A,B). The second external aldimine forms with a rate dependence that indicates a bimolecular reaction (6.2×10^3 M^{-1} s^{-1}) and suggests that **6** interacts with *h*OAT in at least two ways, resulting in parallel reaction paths (Figure 7A,B). The intensity of the combined external aldimine spectra decays partially with the accumulation of a spectral transition characteristic for a quinonoid species (~560 nm) at 0.4 s^{-1} (Figures 7C and 8A,B). The apparent quinonoid species is formed with concomitant and partial decay of the external aldimine transitions that are approximately equal in amplitude to that gained with the second external aldimine accumulation. This suggests that these species reside on the same reaction pathway.

It has been reported that the deprotonation of initial external aldimine **M1** and stepwise fluoride elimination steps proposed in Scheme 6 are typically considered as an E1cB elimination mechanism.[31,32] The electron-withdrawing effect of fluorine and the protonated nitrogen of the aldimine may stabilize the formed carbanion state during the elimination reaction.[32,33]

https://doi.org/10.1021/jacs.1c02456
J. Am. Chem. Soc. 2021, 143, 8689−8703

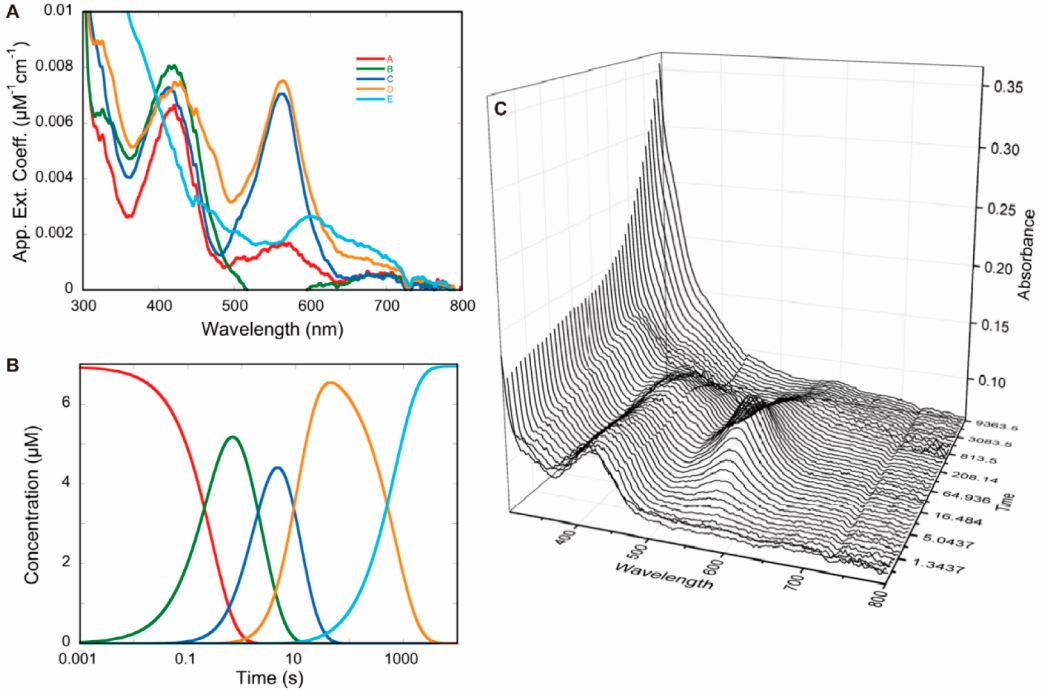

Figure 8. Partial deconvolution by singular value decomposition (SVD) of transient state absorption changes observed for *h*OAT reacting with **6**. *h*OAT (6.94 μM; final concentration) was allowed to react in a stopped-flow spectrophotometer with **6** (1040 μM; final concentration) at 10 °C. To obtain a time resolution sufficient to analyze kinetic rates spanning 4 orders of magnitude, a composite CCD absorbance data set was prepared spanning 250−800 nm and 0.0137−9843 s by splicing together averaged short and long time frame data sets. These data were fit to a linear irreversible four-step model in which the rate constants were constrained to those determined from single-wavelength analyses (Figure 7). (A) Deconvoluted composite spectra were derived from SVD analysis. (B) Species concentration profile based on the rate constants was used to fit the data set. (C) Three-dimensional depiction of a subset of spectra from the data set was analyzed.

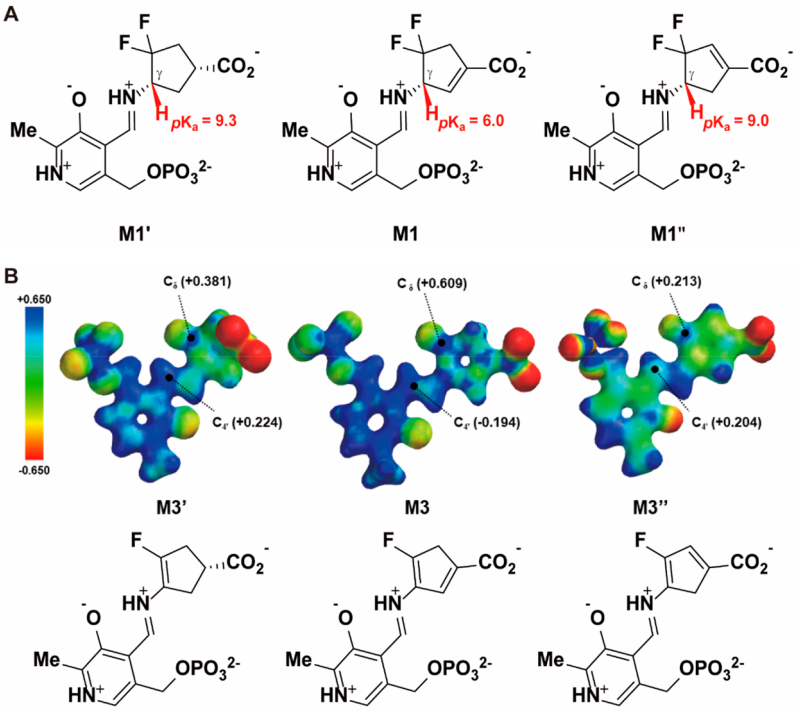

Figure 9. (A) Theoretical pK_a calculations of the hydrogen at the C_γ position using the DFT/B3LYP method and (B) electron density maps colored coded to the electrostatic potential of intermediates and ESP charges of C_δ and $C_{4'}$ positions.

Quinonoid transient state **M2** is expected to form between the first and second external aldimines (**M1** and **M3**). However, the stopped-flow experimental results suggest that the antiperiplanar hydrogen and fluorine atoms in **M1** undergo a Lys292-assisted E2 mechanism,[31] i.e., concerted loss of a proton fluoride ion, with the formation of the alkene as a more

https://doi.org/10.1021/jacs.1c02456
J. Am. Chem. Soc. 2021, 143, 8689−8703

favorable fluoride ion elimination pathway, affording the second external aldimine (**M3**) directly as the single transient state species (*Pathway e*; Scheme 6). This E2 elimination pathway has never been observed experimentally in previous mechanistic studies of other related PLP-dependent aminotransferase inactivators.[1,8]

Assuming a quinonoid extinction coefficient of ∼30 mM^{-1} cm^{-1},[9] the fractional accumulation of the quinonoid observed is ∼20% of the total reacting species at 1 mM **6**. The quinonoid then decays at a rate of 0.09 s^{-1}, while the residual transitions assigned to the external aldimine species broaden and persist (orange spectrum, Figure 8A,B). Quinonoid **M6** seems to be a rare case of quinonoid species (∼560 nm) that can be observed on the basis of the turnover (*Pathway a*; Scheme 5) and inactivation (*Pathway b*; Scheme 6) mechanisms. The final phase observed occurs with a rate constant of 0.007 s^{-1}; in this phase, the features of the external aldimine decay with a pronounced increase in absorption intensity at ∼275 nm, indicative of a loss of conjugation (blue spectrum, Figure 8A,B), consistent with *gem*-diamine **M16** and ketimine **M19**, which are proposed as the final products in Scheme 6.

Collectively, these data support a dominant pathway composed of multiple distinct external aldimine species that ultimately decay to a less conjugated product (turnover mechanism; *Pathways e* then *a* to **M10**; Scheme 6) and a second minor pathway that forms an initial external aldimine more slowly but then proceeds through a quinonoid intermediate and decays to also form a nonconjugated product (inactivation mechanism; *Pathways e-b-c* and *d* to **M16** and **M19**, Scheme 6). The data shown in Figure 8C indicate that the proportion of each pathway is dependent on the concentration of **6**. Higher concentrations of **6** diminish the accumulation of the quinonoid species but do not alter the observed rates of accumulation and decay, suggesting that the more rapid and dominant pathway sequesters a larger fraction of enzyme at higher **6** concentrations.

Significance of the Conjugated Alkene of 6. After better understanding the inactivation and turnover mechanisms of **6**, we carried out computational calculations to compare analogues **4**−**6**. Our previous studies have revealed that incorporating an extra double bond into the cyclopentane ring system establishes an α,β-conjugated carboxylate and facilitates the deprotonation step as a result of the increased acidity of the adjunct proton, leading to an enhanced inactivation rate constant.[18,19] In this work, we performed theoretical pK_a calculations using the DFT/B3LYP method[34] at 298 K to predict the proton's acidity at the C_γ position of difluoro analogues **4**−**6** (Figure 3). The results shown in Figure 9A suggest that the hydrogen (highlighted with red) of PLP-bound **6** (**M1**) with an α, β-conjugated carboxylate system displays the lowest pK_a value among the three analogues, while the pK_a value of the corresponding proton in PLP-bound **5** (**M1″**) is not noticeably affected by the introduced double bond at the C_α and C_ε positions relative to the parent cyclopentane **4** (**M1′**). Taken together with their distinct k_{inact} values (Table 1), our findings suggest that the more acidic hydrogen at the C_γ position facilitates the first external aldimine of **6** (**M1**), which initiates an E2 fluoride ion elimination step rather than the typical E1cB elimination reaction, thus contributing to its enhanced rate constant.

The partition ratio determination and fluoride ion release results (Table 1) elucidated that **4** and **5** predominantly participate in the alternative turnover pathway rather than the inactivation pathway, simultaneously releasing large amounts of fluoride ions. The electron density maps and ESP charge calculations[13] (Figure 9B) indicate that the electrophilicity of C_δ in the transient state **M3** of **6** is much higher than that in the corresponding transient states of **4** and **5** (**M3′** for **4** and **M3″** for **5**), suggesting that the C_δ position of **M3** is more reactive than in the other two intermediates. The $C_{4'}$ positions in the aldimine linkage of **M3′** and **M3″** display comparable electrophilicity that is much greater than that of **M3**, which demonstrates that **M3′** and **M3″** are easier to be attacked by catalytic Lys292 to trigger their turnover pathways, eventually resulting in significant partition ratios for **4** and **5**. Furthermore, additional MS-base analyses in *h*OAT revealed that, similar to **6** in *h*OAT, cyclopentene analogue **5** generated a ketone bearing a single fluorine atom as its primary metabolite (**M5-1**, Figure S7B). In contrast, cyclopentane **4** not only formed a monofluorinated ketone (**M4-1**, Figure S7A) but also generated a ketone metabolite bearing a hydroxyl group (**M4-2**, Figure S7A), which was not detected in the MS-base analyses of cyclopentene analogues. According to the proposed mechanisms for **6** in Scheme 6, it is likely that the incorporated double bond also plays a critical role in stabilizing the conjugated system.

CONCLUSION

Previously, we discovered (*S*)-3-amino-4,4-difluorocyclohex-1-enecarboxylic acid (WZ-2-051, **2**), which inactivates *h*OAT through a covalent addition-aromatization mechanism (Scheme 1 B). However, it also exhibited the apparent inhibition of GABA-AT. In this work, (*S*)-3-amino-4,4-difluorocyclopent-1-enecarboxylic acid (SS-1-148, **6**) exhibited comparable inactivation efficiency to that of preclinical stage selective *h*OAT inactivator $BisCF_3$ (**1**) but was demonstrated to be a reversible inhibitor of GABA-AT. The kinetic studies and computational calculations provide evidence to support the notion that the conjugated alkene of **6** in its cyclopentene ring is essential for retaining high *h*OAT inactivation efficiency. A soaking experiment was performed to obtain a quasi-stable *gem*-diamine intermediate covalently bound to Lys292 in the soaked crystal, an intermediate that has never been captured in other studies of related aminotransferase inactivators. The co-crystallization of *h*OAT and **6** captured a stable noncovalent final product in the *h*OAT co-crystal complex. The critical salt bridge of Arg413-Glu235 in *h*OAT was found to be broken in both crystal complexes. In addition, we have applied native MS, for the first time, in studies of aminotransferase inactivators to further support the noncovalent pathway as the primary inactivation mechanism of **6**. We also performed intact MS to support a covalent modification observed as a minor form, which appears to be a *gem*-diamine structure in equilibrium with the noncovalent form. Using rapid-mixing experiments, we observed, for the first time, that the first external aldimine of **6** undergoes a lysine-assisted E2 fluoride ion elimination instead of the typical E1cB elimination mechanism, forming the second external aldimine as the single transient state. Overall, we have carried out comprehensive mechanistic studies to demonstrate that **6** mainly inactivates *h*OAT through a noncovalent water-mediated mechanism. However, it is still unclear why there are distinct inactivation mechanisms for cyclopentene **6** and the corresponding cyclohexene **2**.

https://doi.org/10.1021/jacs.1c02456
J. Am. Chem. Soc. 2021, 143, 8689−8703

■ ASSOCIATED CONTENT

Supporting Information

The Supporting Information is available free of charge at https://pubs.acs.org/doi/10.1021/jacs.1c02456.

Figures of linear regression analysis, time-dependent dialysis, Polder maps, MS spectra, Gibb's free energy, tautomeric forms, primary metabolites, NMR spectra, and HRMS report, scheme of theoretical pK_a calculations, tables of statistics of crystal structures, and discussions of synthetic methods, expression and purification of *h*OAT, aminotransferases and coenzymes for kinetic studies, evaluation of compounds as time-dependent inhibitors of *h*OAT, evaluation of compounds as reversible inhibitors of GABA-AT, inhibition of Asp-AT and Ala-AT by **6**, dialysis assay, partition ratio experiment, fluoride ion release assay, native protein mass spectrometry, denaturing intact protein and small molecule mass spectrometry, crystallization and crystal soaking of *h*OAT with **6**, transient state methods, Gibb's free energy calculation, theoretical pK_a calculations, and ESP charge calculation (PDF)

Accession Codes

Atomic coordinates and corresponding structure factors for the soaking result and co-crystal complex have been deposited at the Protein Data Bank (PDB) as the 7LK1 and 7LK0 entries, respectively. Authors will release the atomic coordinates upon article publication.

■ AUTHOR INFORMATION

Corresponding Authors

Dali Liu − *Department of Chemistry and Biochemistry, Loyola University Chicago, Chicago, Illinois 60660, United States;* orcid.org/0000-0002-7587-703X; Phone: +1-773-508-3093; Email: dliu@luc.edu

Richard B. Silverman − *Department of Chemistry, Center for Molecular Innovation and Drug Discovery, and Center for Developmental Therapeutics and Department of Molecular Biosciences, Northwestern University, Evanston, Illinois 60208, United States; Department of Pharmacology, Northwestern University, Chicago, Illinois 60611, United States;* orcid.org/0000-0001-9034-1084; Phone: +1-847-491-5653; Email: r-silverman@northwestern.edu

Authors

Sida Shen − *Department of Chemistry, Center for Molecular Innovation and Drug Discovery, and Center for Developmental Therapeutics, Northwestern University, Evanston, Illinois 60208, United States;* orcid.org/0000-0002-0295-2545

Arseniy Butrin − *Department of Chemistry and Biochemistry, Loyola University Chicago, Chicago, Illinois 60660, United States*

Peter F. Doubleday − *Department of Molecular Biosciences, Northwestern University, Evanston, Illinois 60208, United States;* Present Address: P.F.D.: Institute of Molecular Systems Biology, ETH Zurich, 8093 Zurich, Switzerland.

Rafael D. Melani − *Department of Molecular Biosciences, Northwestern University, Evanston, Illinois 60208, United States*

Brett A. Beaupre − *Department of Chemistry and Biochemistry, Loyola University Chicago, Chicago, Illinois 60660, United States*

Mauricio T. Tavares − *Department of Molecular Medicine, Scripps Research, Jupiter, Florida 33458, United States*

Glaucio M. Ferreira − *Department of Clinical and Toxicological Analyses, School of Pharmaceutical Sciences, University of São Paulo, São Paulo, SP 05508-000, Brazil;* orcid.org/0000-0002-1952-9428

Neil L. Kelleher − *Department of Chemistry, Center for Molecular Innovation and Drug Discovery, and Center for Developmental Therapeutics and Department of Molecular Biosciences, Northwestern University, Evanston, Illinois 60208, United States;* orcid.org/0000-0002-8815-3372

Graham R. Moran − *Department of Chemistry and Biochemistry, Loyola University Chicago, Chicago, Illinois 60660, United States;* orcid.org/0000-0002-6807-1302

Complete contact information is available at: https://pubs.acs.org/10.1021/jacs.1c02456

Author Contributions

[▽]S.S. and A.B. contributed equally to this paper.

Notes

The authors declare no competing financial interest.

■ ACKNOWLEDGMENTS

The authors are grateful to the National Institutes of Health (Grant R01 DA030604 to R.B.S. and Grant P30 DA018310 to N.L.K.) and National Science Foundation (Grant 2015210477 to P.F.D. and Grant 1904480 to G.R.M.) for financial support. This work used the Extreme Science and Engineering Discovery Environment (XSEDE) Comet Bridges Stampede2 through allocation TG-CHE190070, which is supported by National Science Foundation grant number ACI-1548562. This work made use of the IMSERC at Northwestern University, which has received support from the Soft and Hybrid Nanotechnology Experimental (SHyNE) Resource (NSF NNCI-1542205), the State of Illinois, and the International Institute for Nanotechnology (IIN). X-ray diffraction data collection used resources of the Advanced Photon Source, a U.S. Department of Energy (DOE) Office of financial support. Science User Facility was operated for the DOE Office of Science by Argonne National Laboratory under contract no. DEAC02-06CH11357. The use of LS-CAT Sector 21 was supported by the Michigan Economic Development Corporation and the Michigan Technology Tri-Corridor (grant 085P1000817). G.M.F. is a recipient of a fellowship from FAPESP, Brazil. The authors would also like to thank Drs. Wei Zhu and Pathum M. Weerawarna for constructive comments and revision.

■ ABBREVIATIONS

AFPA, (*S*)-4-amino-5-fluoropentanoic acid; Boc_2O, di-*tert*-butyl dicarbonate; Deoxo-Fluor, bis(2-methoxyethyl)-aminosulfur trifluoride; DMPK, drug metabolism and pharmacokinetics; DIPEA, *N*,*N*-diisopropylethylamine; DBDMH, 1,3-dibromo-5,5-dimethylhydantoin; DMF, dimethylformamide; DMSO, dimethyl sulfoxide; DCM, dichloromethane; KHMDS, potassium bis(trimethylsilyl)amide; PO, per os administration; THF, tetrahydrofuran; TEA, triethylamine; TBAI, tetra-*n*-butylammonium iodide

https://doi.org/10.1021/jacs.1c02456
J. Am. Chem. Soc. 2021, 143, 8689−8703

REFERENCES

(1) Lee, H.; Juncosa, J. I.; Silverman, R. B. Ornithine aminotransferase versus GABA aminotransferase: implications for the design of new anticancer drugs. *Med. Res. Rev.* **2015**, *35*, 286−305.

(2) Tanner, J. J.; Fendt, S. M.; Becker, D. F. The proline cycle as a potential cancer therapy target. *Biochemistry* **2018**, *57*, 3433−3444.

(3) Tang, L.; Zeng, J.; Geng, P.; Fang, C.; Wang, Y.; Sun, M.; Wang, C.; Wang, J.; Yin, P.; Hu, C.; Guo, L.; Yu, J.; Gao, P.; Li, E.; Zhuang, Z.; Xu, G.; Liu, Y. Global metabolic profiling identifies a pivotal role of proline and hydroxyproline metabolism in supporting hypoxic response in hepatocellular carcinoma. *Clin. Cancer Res.* **2018**, *24*, 474−485.

(4) Cadoret, A.; Ovejero, C.; Terris, B.; Souil, E.; Levy, L.; Lamers, W. H.; Kitajewski, J.; Kahn, A.; Perret, C. New targets of beta-catenin signaling in the liver are involved in the glutamine metabolism. *Oncogene* **2002**, *21*, 8293−8301.

(5) Llovet, J. M.; Zucman-Rossi, J.; Pikarsky, E.; Sangro, B.; Schwartz, M.; Sherman, M.; Gores, G. Hepatocellular carcinoma. *Nat. Rev. Dis. Primers.* **2016**, *2*, 16018.

(6) Zigmond, E.; Ya'acov, A. B.; Lee, H.; Lichtenstein, Y.; Shalev, Z.; Smith, Y.; Zolotarov, L.; Ziv, E.; Kalman, R.; Le, H. V.; Lu, H.; Silverman, R. B.; Ilan, Y. Suppression of hepatocellular carcinoma by inhibition of overexpressed ornithine aminotransferase. *ACS Med. Chem. Lett.* **2015**, *6*, 840−844.

(7) Eliot, A. C.; Kirsch, J. F. Pyridoxal phosphate enzymes: mechanistic, structural, and evolutionary considerations. *Annu. Rev. Biochem.* **2004**, *73*, 383−415.

(8) Silverman, R. B. Design and mechanism of GABA aminotransferase inactivators. Treatments for epilepsies and addictions. *Chem. Rev.* **2018**, *118*, 4037−4070.

(9) Butrin, A.; Beaupre, B. A.; Kadamandla, N.; Zhao, P.; Shen, S.; Silverman, R. B.; Moran, G. R.; Liu, D. Structural and kinetic analyses reveal the dual inhibition modes of ornithine aminotransferase by (1S,3S)-3-amino-4-(hexafluoropropan-2-ylidenyl)-cyclopentane-1-carboxylic acid (BCF3). *ACS Chem. Biol.* **2021**, *16*, 67−75.

(10) Pan, Y.; Gerasimov, M. R.; Kvist, T.; Wellendorph, P.; Madsen, K. K.; Pera, E.; Lee, H.; Schousboe, A.; Chebib, M.; Brauner-Osborne, H.; Craft, C. M.; Brodie, J. D.; Schiffer, W. K.; Dewey, S. L.; Miller, S. R.; Silverman, R. B. (1S, 3S)-3-amino-4-difluoromethylenyl-1-cyclopentanoic acid (CPP-115), a potent gamma-aminobutyric acid aminotransferase inactivator for the treatment of cocaine addiction. *J. Med. Chem.* **2012**, *55*, 357−366.

(11) Copeland, R. A. *Evaluation of enzyme inhibitors in drug discovery: A guide for medicinal chemists and pharmacologists*; Wiley-Interscience, 2005; pp 1−265.

(12) Moschitto, M. J.; Doubleday, P. F.; Catlin, D. S.; Kelleher, N. L.; Liu, D.; Silverman, R. B. Mechanism of inactivation of ornithine aminotransferase by (1S,3S)-3-amino-4-(hexafluoropropan-2-ylidenyl)cyclopentane-1-carboxylic acid. *J. Am. Chem. Soc.* **2019**, *141*, 10711−10721.

(13) Zhu, W.; Doubleday, P. F.; Catlin, D. S.; Weerawarna, P. M.; Butrin, A.; Shen, S.; Wawrzak, Z.; Kelleher, N. L.; Liu, D.; Silverman, R. B. A remarkable difference that one fluorine atom confers on the mechanisms of inactivation of human ornithine aminotransferase by two cyclohexene analogues of gamma-aminobutyric acid. *J. Am. Chem. Soc.* **2020**, *142*, 4892−4903.

(14) Daune, G.; Gerhart, F.; Seiler, N. 5-Fluoromethylornithine, an irreversible and specific inhibitor of L-ornithine:2-oxo-acid aminotransferase. *Biochem. J.* **1988**, *253*, 481−488.

(15) Bolkenius, F. N.; Knodgen, B.; Seiler, N. DL-canaline and 5-fluoromethylornithine. Comparison of two inactivators of ornithine aminotransferase. *Biochem. J.* **1990**, *268*, 409−414.

(16) Storici, P.; Capitani, G.; Muller, R.; Schirmer, T.; Jansonius, J. N. Crystal structure of human ornithine aminotransferase complexed with the highly specific and potent inhibitor 5-fluoromethylornithine. *J. Mol. Biol.* **1999**, *285*, 297−309.

(17) Qiu, J.; Silverman, R. B. A new class of conformationally rigid analogues of 4-amino-5-halopentanoic acids, potent inactivators of gamma-aminobutyric acid aminotransferase. *J. Med. Chem.* **2000**, *43*, 706−720.

(18) Juncosa, J. I.; Takaya, K.; Le, H. V.; Moschitto, M. J.; Weerawarna, P. M.; Mascarenhas, R.; Liu, D.; Dewey, S. L.; Silverman, R. B. Design and mechanism of (S)-3-amino-4-(difluoromethylenyl)cyclopent-1-ene-1-carboxylic acid, a highly potent gamma-aminobutyric acid aminotransferase inactivator for the treatment of addiction. *J. Am. Chem. Soc.* **2018**, *140*, 2151−2164.

(19) Shen, S.; Doubleday, P. F.; Weerawarna, P. M.; Zhu, W.; Kelleher, N. L.; Silverman, R. B. Mechanism-based design of 3-amino-4-halocyclopentenecarboxylic acids as inactivators of GABA aminotransferase. *ACS Med. Chem. Lett.* **2020**, *11*, 1949−1955.

(20) Singh, R.; Vince, R. 2-Azabicyclo[2.2.1]hept-5-en-3-one: chemical profile of a versatile synthetic building block and its impact on the development of therapeutics. *Chem. Rev.* **2012**, *112*, 4642−4686.

(21) Wang, B. L.; Gao, H. T.; Li, W. D. Total synthesis of (+)-iresin. *J. Org. Chem.* **2015**, *80*, 5296−5301.

(22) Gross, L. J.; Stark, C. B. W. Regioselective dehydration of alpha-hydroxymethyl tetrahydrofurans using Burgess' reagent under microwave irradiation. *Org. Biomol. Chem.* **2017**, *15*, 4282−4285.

(23) Lee, H.; Doud, E. H.; Wu, R.; Sanishvili, R.; Juncosa, J. I.; Liu, D.; Kelleher, N. L.; Silverman, R. B. Mechanism of inactivation of gamma-aminobutyric acid aminotransferase by (1S,3S)-3-amino-4-difluoromethylene-1-cyclopentanoic acid (CPP-115). *J. Am. Chem. Soc.* **2015**, *137*, 2628−2640.

(24) Mascarenhas, R.; Le, H. V.; Clevenger, K. D.; Lehrer, H. J.; Ringe, D.; Kelleher, N. L.; Silverman, R. B.; Liu, D. Selective targeting by a mechanism-based inactivator against pyridoxal 5′-phosphate-dependent enzymes: mechanisms of inactivation and alternative turnover. *Biochemistry* **2017**, *56*, 4951−4961.

(25) Di Salvo, M. L.; Scarsdale, J. N.; Kazanina, G.; Contestabile, R.; Schirch, V.; Wright, H. T. Structure-based mechanism for early PLP-mediated steps of rabbit cytosolic serine hydroxymethyltransferase reaction. *BioMed Res. Int.* **2013**, *2013*, 458571.

(26) Soniya, K.; Awasthi, S.; Nair, N. N.; Chandra, A. Transimination reaction at the active site of aspartate aminotransferase: a proton hopping mechanism through pyridoxal 5′-phosphate. *ACS Catal.* **2019**, *9*, 6276−6283.

(27) Shah, S. A.; Shen, B. W.; Brunger, A. T. Human ornithine aminotransferase complexed with L-canaline and gabaculine: structural basis for substrate recognition. *Structure* **1997**, *5*, 1067−1075.

(28) Stewart, J. J. MOPAC: a semiempirical molecular orbital program. *J. Comput.-Aided Mol. Des.* **1990**, *4*, 1−105.

(29) Karsten, W. E.; Ohshiro, T.; Izumi, Y.; Cook, P. F. Reaction of serine-glyoxylate aminotransferase with the alternative substrate ketomalonate indicates rate-limiting protonation of a quinonoid intermediate. *Biochemistry* **2005**, *44*, 15930−15936.

(30) Thibodeaux, C. J.; Liu, H. W. Mechanistic studies of 1-aminocyclopropane-1-carboxylate deaminase: characterization of an unusual pyridoxal 5′-phosphate-dependent reaction. *Biochemistry* **2011**, *50*, 1950−1962.

(31) Clift, M. D.; Ji, H.; Deniau, G. P.; O'Hagan, D.; Silverman, R. B. Enantiomers of 4-amino-3-fluorobutanoic acid as substrates for gamma-aminobutyric acid aminotransferase. Conformational probes for GABA binding. *Biochemistry* **2007**, *46*, 13819−13828.

(32) Gokcan, H.; Konuklar, F. A. Theoretical study on HF elimination and aromatization mechanisms: a case of pyridoxal 5′ phosphate-dependent enzyme. *J. Org. Chem.* **2012**, *77*, 5533−5543.

(33) Alunni, S.; De Angelis, F.; Ottavi, L.; Papavasileiou, M.; Tarantelli, F. Evidence of a borderline region between E1cb and E2 elimination reaction mechanisms: a combined experimental and theoretical study of systems activated by the pyridine ring. *J. Am. Chem. Soc.* **2005**, *127*, 15151−15160.

(34) Ghalami-Choobar, B.; Dezhampanah, H.; Nikparsa, P.; Ghiami-Shomami, A. Theoretical calculation of the pKa values of some drugs in aqueous solution. *Int. J. Quantum Chem.* **2012**, *112*, 2275−2280.

https://doi.org/10.1021/jacs.1c02456
J. Am. Chem. Soc. 2021, 143, 8689−8703